Selenium@Mesoporous Carbon Composite with Superior Lithium and Sodium Storage Capacity

Chao Luo,[†] Yunhua Xu,[†] Yujie Zhu, Yihang Liu, Shiyou Zheng, Ying Liu, Alex Langrock, and Chunsheng Wang*

Department of Chemical and Biomolecular Engineering, University of Maryland, College Park, Maryland 20742, United States. [†]These authors contributed to this work equally.

ABSTRACT Selenium-impregnated carbon composites were synthesized by infusing Se into mesoporous carbon at a temperature of 600 °C under vacuum. Ring-structured Se_8 was produced and confined in the mesoporous carbon, which acts as an electronic conductive matrix. During the electrochemical process in low-cost $LiPF_6$/EC/DEC electrolyte, low-order polyselenide intermediates formed and were stabilized by mesoporous carbon, which avoided the shuttle reaction of polyselenides. Exceptional electrochemical performance of Se/mesoporous carbon composites was demonstrated in both Li-ion and Na-ion batteries. In lithium-ion batteries, Se_8/mesoporous carbon composite cathodes delivered a reversible capacity of 480 mAh g^{-1} for 1000 charge/discharge cycles without any capacity loss, while in Na-ion batteries, it provided initial capacity of 485 mAh g^{-1} and retained 340 mAh g^{-1} after 380 cycles. The Se_8/mesoporous carbon composites also showed excellent rate capability. As the current density increased from 0.1 to 5 C, the capacity retained about 46% in Li-ion batteries and 34% in Na-ion batteries.

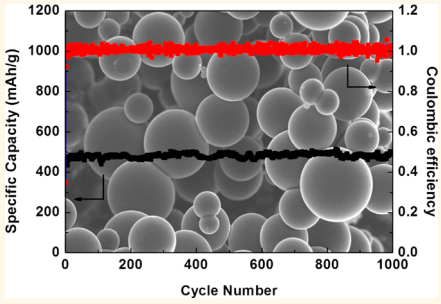

KEYWORDS: selenium cathode · mesoporous carbon · lithium-ion batteries · sodium-ion batteries · polyselenides · shuttle effect

High-energy lithium-ion batteries and low-cost sodium-ion batteries are the most promising candidates for emerging electric vehicles and large-scale renewable energy storage, respectively. In current technology, the energy density of lithium-ion batteries is mainly limited by the cathode material.[1−3] The same problem also impedes the development of sodium-ion batteries.[4] Therefore, development of high-energy density cathodes for both Li-ion and Na-ion batteries is critical for the success in electric vehicle and renewable energy storage.

Sulfur is the only cathode material that has comparable capacity with the Si anode material for Li-ion batteries. However, sulfur cathodes face three major challenges, which limit its practical applications:[5−7] (1) sulfur has low electronic conductivity; (2) sulfur undergoes large volume change during lithiation/delithiation; (3) high-order polysulfide intermediates are soluble in carbonate electrolytes. The dissolution of high-order polysulfides is essential for progressive lithiation of S_8 due to the nonconductive nature of elemental S_8 and its reduction products.[8] However, the dissolved high-order polysulfides also cause a shuttle reaction because dissolved high-order polysulfides in the cathode side can diffuse to and chemically react with the Li anode to either form soluble low-order polysulfides and then transport back to cathode side, causing a shuttle reaction, or form an insoluble dense sulfides (Li_2S and Li_2S_2) layer on the Li anode, increasing the resistance of the Li anode. The shuttle reaction and deposition of Li_2S on the Li anode significantly reduce Coulombic efficiency and cycle stability of sulfur cathodes for both lithium− and sodium−sulfur batteries.[9,10] Most effective ways to alleviate dissolution and shuttle reaction are (1) to physically trap the high-order polysulfides inside host materials (mostly conductive carbon),[11−13] (2) to directly form insoluble low-order sulfides,[14] and (3) to manipulate the solubility of polysulfides by selection of different electrolytes.[15,16] Our previous work showed that small sulfur molecules obtained at a high temperature

* Address correspondence to cswang@umd.edu.

Received for review June 19, 2013 and accepted August 14, 2013.

Published online August 14, 2013
10.1021/nn403108w

(500 °C) can be infused into carbon nanotubes and stabilized to room temperature.[6] The small sulfur/carbon nanotube composite can directly form insoluble low-order polysulfides, thus avoiding the dissolution and shuttle reaction.

As a congener of sulfur, selenium has similar chemical properties but higher electronic conductivity. Selenium can also react with lithium and sodium ions to generate selenides.[17] Although the gravimetric capacity of the selenium cathode (678 mAh g^{-1}) is lower than that of sulfur (1672 mAh g^{-1}), the volumetric capacity of selenium (3253 Ah L^{-1} based on 4.82 g cm^{-3}) is comparable to that of sulfur (3467 Ah L^{-1} based on 2.07 g cm^{-3}). In addition, selenium has 20 orders of magnitude higher electrical conductivity than sulfur. These features make it a promising cathode material for both lithium- and sodium-ion batteries. However, similar to sulfur, the selenium cathodes also face the dissolution issue of high-order polyselenides, resulting in fast capacity fading and low Coulombic efficiency.

In this study, using the same strategy of S/C cathode in Li–sulfur batteries, we broke Se_{12} into Se_8 at a high temperature of 600 °C and impregnated Se_8 into mesoporous carbon to alleviate the dissolution of polyselenides. The Se_8/C cathode in carbonate-based electrolyte demonstrated excellent electrochemical performance in both Li-ion and Na-ion batteries. It can deliver reversible capacity of 480 mAh g^{-1} in lithium-ion batteries and maintains 1000 cycles without any capacity loss. The capacity of the Se/C composite for sodium-ion batteries is as high as 485 mAh g^{-1} in the first cycle and retains 340 mAh g^{-1} after 380 cycles. The Se_8/mesoporous carbon composites also show excellent rate capability. As the current density increased from 0.1 to 5 C, the capacity retained about 46% in Li-ion batteries and 34% in Na-ion batteries. The charge/discharge mechanism of Se_8/C was investigated by comparing the electrochemical behavior of Se_8/C with 1 M $LiPF_6$ in a mixture of ethylene carbonate/diethyl carbonate (EC/DEC, 1:1 by volume) and 1 M LiTFSI in tetraethylene glycol dimethyl ether (TEGDME) electrolytes. The excellent battery performance of Li–Se and Na–Se batteries demonstrates that selenium is a promising alternative to sulfur and currently used cathode materials for large-scale and high-energy applications.

RESULTS AND DISCUSSION

Figure 1a shows the SEM image of the mesoporous carbon. The mesoporous carbon has a spherical morphology with a particle size of a couple of micrometers. The Brunauer–Emmett–Teller (BET) analysis shows that mesoporous carbon has high porosity of 0.2 cm^3 g^{-1} and large surface area of 462 m^2 g^{-1}. The average pore size in mesoporous carbon is about 1.6 nm.

As revealed in Figure 1b, no morphology change is observed after selenium is infused into the mesoporous carbon spheres, suggesting that most of the Se is filled inside the mesoporous carbon. The infusion of Se into the mesopores of carbon is confirmed by the drastic decrease in surface area from 462 m^2 g^{-1} for as-prepared samples to 5 m^2 g^{-1} after Se infusion, while the average pore size increases from 1.6 to 4.1 nm, indicating that small pores are occupied by Se. The elemental mapping images (Figure 1d,e) reveal that selenium is uniformly distributed in the mesopores of carbon spheres. It is also confirmed by the XRD pattern that selenium in mesoporous carbon maintains its crystal structure (JCPDS File No. 86-2246). Thermogravimetric analysis (Supporting Information Figure S1) shows that the porous C/Se composite contains 30% selenium and 70% mesoporous carbon spheres.

The nature of Se in the composite was investigated by Raman spectroscopy. For comparison, porous carbon, pristine Se, and Se treated at 600 °C under the same conditions as those used for Se/C composite were also analyzed (Figure 2). The pristine Se displays three peaks at 142, 235, and 458 cm^{-1}, respectively. The peaks at 142 and 458 cm^{-1} represent Se_{12} with a ring structure,[18] while the 235 cm^{-1} peak is attributed to chain-structured Se,[19] indicating that the pristine Se is a mixture of ring-structured Se_{12} and chain-structured Se molecules. To examine the effects of the heat-treatment history on the structure of Se, the pristine Se was heat-treated using the same procedure used for the Se/C composite. Compared with the nontreated Se, there is no change in Raman spectra, indicating that the mixture of ring- and chain-structured Se is a thermodynamically stable form at room temperature. However, the Se/C composite synthesized at 600 °C in vacuum does not show these three peaks. Instead, a peak at 262 cm^{-1} which is assigned to the ring-structured Se_8 appears.[20] Therefore, the ring-structured Se_8 is stabilized by porous carbon at room temperature. Two strong peaks at 1350 and 1600 cm^{-1} which represent the D and G bands of mesoporous carbon, respectively, are observed for the composite, showing that the porous carbon is partially graphitized. The Raman spectra reveal that the mesopores of carbon can physically restrict Se in the form of small molecules of Se_8, which is similar to sulfur in the S/porous carbon composite.[14]

The electrochemical performance of the Se/C composite cathodes was examined for both lithium- and sodium-ion batteries using conventional carbonate-based electrolyte. Figure 3 shows cyclic voltammograms (CV) and charge/discharge profiles of Se/C composite cathodes in Li-ion and Na-ion batteries. The CV curves show only one pair of reversible redox peaks for both lithium– and sodium–selenium batteries, indicating that the electrochemical process is a single phase-change reaction. For lithium–selenium batteries, cathodic peak and anodic peak appear at 1.1

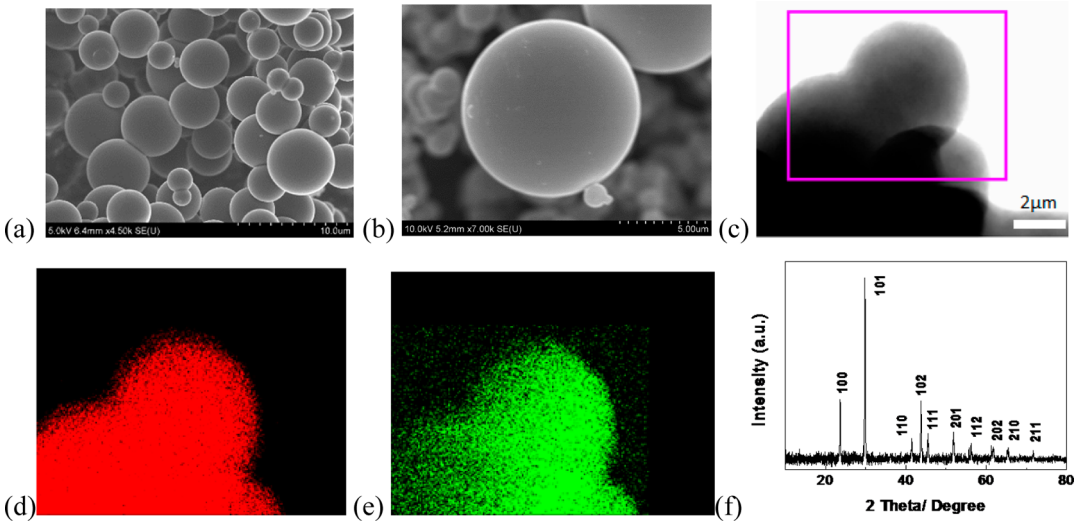

Figure 1. (a) SEM images of mesoporous carbon spheres and (b) Se/C composite. (c) TEM image of selenium-impregnated carbon composite; elemental mapping images of the Se/C composite: Se (d) and carbon (e). (f) XRD pattern of the Se/C composite.

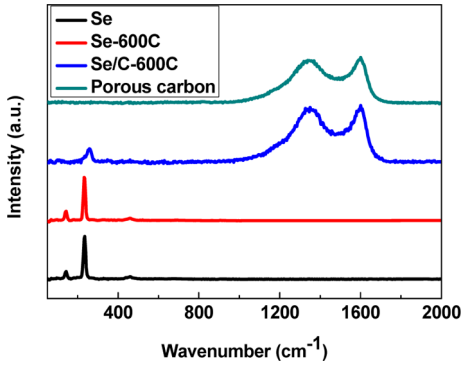

Figure 2. Raman spectra of pristine Se, heat-treated Se, Se/C composite, and porous carbon.

and 1.8 V, respectively, in the first cycle. After the first cycle, the cathodic peak shifts to a higher voltage of 1.4 V, while the anodic peak remains at 1.8 V. Therefore, there is an electrochemical activation process during the first lithiation. This activation process is associated with the deformation of the Se/C composite induced by the volume increase in the first lithiation. Similar phenomena have been reported in high-capacity Si, MnO_x, and other high-capacity anode materials.[21,22] The stable anodic and cathodic peaks after the first cycle demonstrate good cycling stability of the Se/C composite. Figure 3b shows that the CV curves of the Se/C composite in Na−Se batteries measured at a scan rate of 0.1 mV/s between 0.5 and 2.5 V. The Se/C composite in Na−Se batteries also shows activation behavior similar to that in Li−Se batteries. The cathodic peak is at 0.7 V in the first cycle and shifts to a higher potential of 1.0 V in subsequent cycles, while the anodic peak at 1.4 V remains constant in all cycles. Therefore, the redox potentials in Na−Se batteries are about 0.4 V lower than those in Li−Se batteries, which is similar to Sn anodes where the potential in Na-ion batteries is also lower than that in Li-ion batteries.[23]

The charge/discharge profiles of Se/C cathodes at a current density of 0.25 C for both Li− and Na−Se batteries are shown in Figure 3c,d, respectively. As demonstrated in CV, ring-structured Se_8 cathodes present only one slope voltage plateau in both Li-ion and Na-ion batteries, which is in agreement with Yang's results using the same electyrolyte.[24] This charge/discharge behavior is different from previous reports on chain-structured Se_{12} cathodes,[17,25] where multiple plateaus were displayed. Therefore, the difference in charge/discharge curves between Se_{12} (a mixture of ring and chain) and Se_8 indicates different reaction mechanisms in different electrolytes. The charge/discharge potentials are 1.8/1.6 V in Li−Se batteries, which are 0.4 V higher than those in Na−Se batteries (1.4/1.2 V).

The (de)lithiation mechanism of the Se cathode in ether-based electrolyte has been reported by Cui *et al.*[25] During the lithiation, Se undergoes a two-phase transition process where Se is first reduced to soluble high-order polyselenide Se_n^{2-} ($n \geq 4$), and then the Se_n^{2-} ($n \geq 4$) is further reduced to Se_2^{2-} and Se^{2-}. During the delithiation, Li_2Se is first oxidized to Se_n^{2-} ($n \geq 4$), and then the high-order polyselenide is further oxidized to Se. The soluble polyselenides Li_2Se_n ($n \geq 4$) in ether-based electrolyte can cause shuttle reaction.[17,25] In our work, we only observe one plateau of Se/C during lithiation/delithiation in carbonate electrolyte, which is in agreement with Yang's results using the same carbonate electrolyte.[24] Yang *et al.* believed that Se/C in carbonate electrolyte only experiences a direct phase change between insoluble chain-structured Se_n to insoluble Li_2Se without formation of soluble lithium polyselenide Li_2Se_n ($n \geq 4$).[24] The

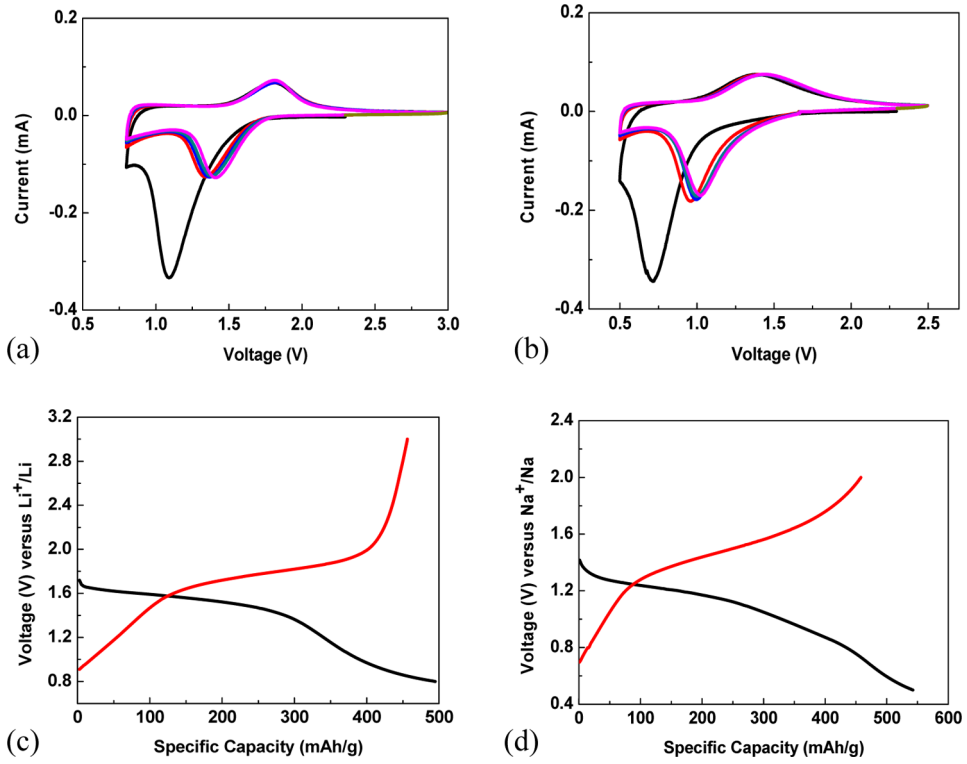

Figure 3. Cyclic voltammograms of the Se/C composite in the initial five cycles *vs* (a) Li and (b) Na. Charge/discharge profiles at the secnd cycle of the Se/C composite in (c) Li-ion and (d) Na-ion batteries.

difference in the lithiation/delithiation mechanism of Se/C between our work and Cui's work is mainly attributed to the use of different electrolyte. The multistep phase transitions of Se/C in ether-based electrolyte but a single-step reaction in carbonate-based electrolyte was also reported by Amine's group.[17,25] Although the carbonyl groups of the carbonate electrolyte can react with Se anions, the mesoporous carbon host reduces this side reaction and the stable Se−O layer formed on Li_xSe protects Li_xSe from further reduction (Se−O layer functions as a SEI) as demonstrated by stable interface impedance during charge/discharge cycles (Figure S2) and long cycling stability (Figure 4).

The cycling stability of the Se/C composite was investigated at a current density of 0.25 C for both Li−Se cells and Na−Se cells (Figure 4). The Se/C composite exhibits exceptional cycling stability in both lithium-ion and sodium-ion batteries. The Li−Se batteries deliver a reversible capacity of 480 mAh g^{-1} in the first cycle, and no capacity decline is observed during 1000 cycles, demonstrating superior cycling performance. The Coulombic efficiency of Li−Se batteries is nearly 100%, demonstrating that the shuttle reaction has been effectively suppressed. It is worth noting that good cycling performance is also obtained for Na−Se cells. Normally, electrodes in Na-ion batteries show much worse reaction kinetics, lower capacity, and poorer cycling stability than in Li-ion batteries due to the larger diameter of sodium ions compared to lithium ions.[26] In this study, the Se/C composite shows similar reversible capacity (485 mAh g^{-1}) in Na-ion cells to that (480 mAh g^{-1}) in Li-ion cells and retains 340 mAh g^{-1} after 380 cycles which corresponds to 70% of its initial capacity.

In addition to the good cycling stability, the Se/C composite also shows high rate capability in both Li-ion and Na-ion batteries. As current density increases from 0.1 to 5 C, the capacity of the Se/C composite in Li−Se batteries only decreases from 500 to 229 mAh g^{-1}, while the capacity of the Se/C composite in Na−Se batteries is reduced from 500 to 168 mAh g^{-1}. The impedances of Se/C cathodes before cycling, and after 50, 100, and 150 cycles are compared in Figure S2. All EISs show a depressed semicircle in the high-frequency region and a slope line in the low-frequency region, which is the same as the impedance of Se/C reported by Cui *et al.*[25] The depressed high-frequency semicircle represents interface impedance (including contact impedance of Se/C particles, or SEI impedance, and charge transfer impedance), while the low-frequency line is attributed to ion diffusion in the Se/C particles. The fresh Se/C cell possesses a small interface resistance of ~100 Ω and increase to 150 Ω at 50 cycles and stabilizes to 150 Ω in the flowing cycles. The initial increase in interface impedance in the first few cycles may be attributed to volume change of Se/C during charge/discharge cycles and side reaction between polyselenides and carbonate electrolyte.[25] The stable interface impedance during charge/discharge cycles

demonstrates that the formation of the Se−O layer on polyselenides protects polyselenides from further side reaction. The low and stable interface resistance of Se/C in the charge/discharge cycles demonstrates that Se/C cathodes have fast reaction kinetics, which has been confirmed by the high rate capability (Figure 4c), while the stable interface resistance of Se/C during charge/discharge cycles is coincident with the long cycling stability (Figure 4a). The exceptional electrochemical performance reveals that the Se/C composite is a promising electrode material for both Li-ion and Na-ion batteries.

The good cycling stability of the Se/C composite is believed to be associated with the unique structure of the Se/C composite. Therefore, the morphology and structure of the Se/C composite electrodes after 1000 cycles in Li−Se batteries are investigated by SEM, XRD (Figure 5), and TEM (Figure S3). Compared to Figure 1, no obvious morphology change is observed after 1000 cycles (Figure 5a), which demonstrates that a robust mesoporous carbon can effectively accommodate the large volume change of Se during lithiation/delithiation. After 1000 cycles, selenium in mesoporous carbon still retains the crystal structure as evidenced by the XRD pattern (Figure 5b). The extra peaks in the XRD pattern may be assigned to the SEI film. The EDS mapping results (Figure S3) show that Se is still uniformly dispersed in porous carbon after 1000 cycles. Similar results are also observed for Na−Se batteries, as shown in Figure S4.

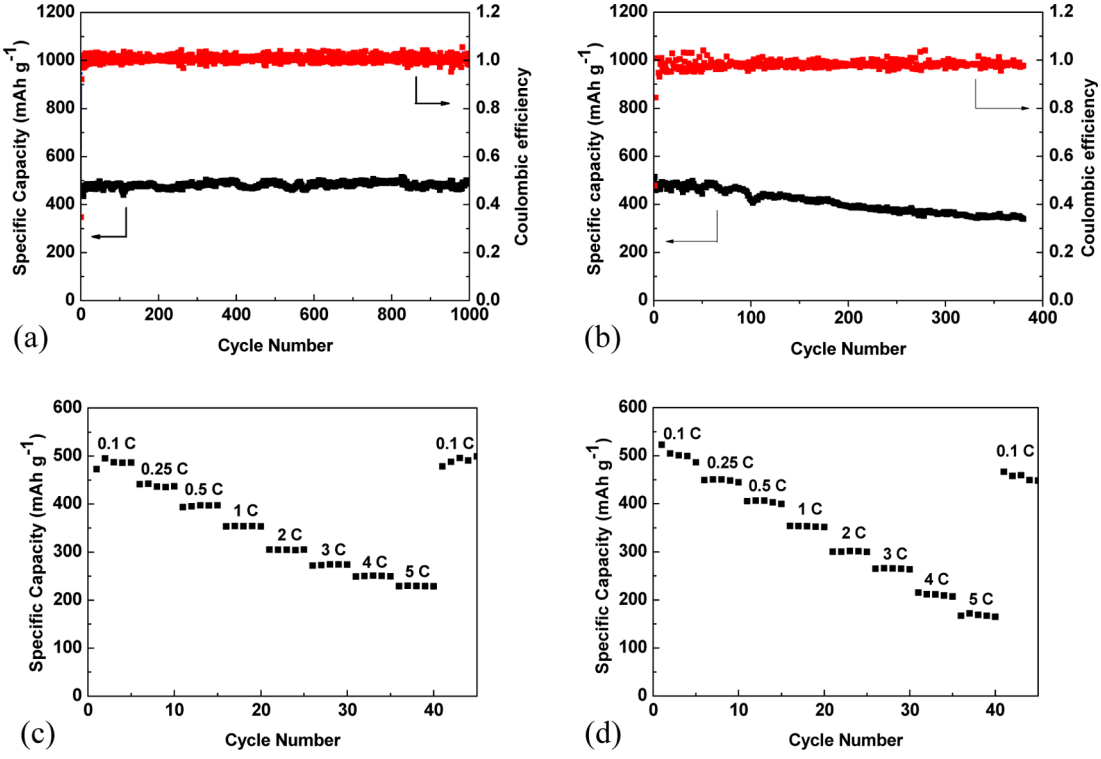

Figure 4. Cycling performance of the Se/C composite in (a) Li-ion and (b) Na-ion batteries. Rate capability of the Se/C composite in (c) Li-ion and (d) Na-ion batteries (1 C is defined as 678 mA g^{-1} based on Se).

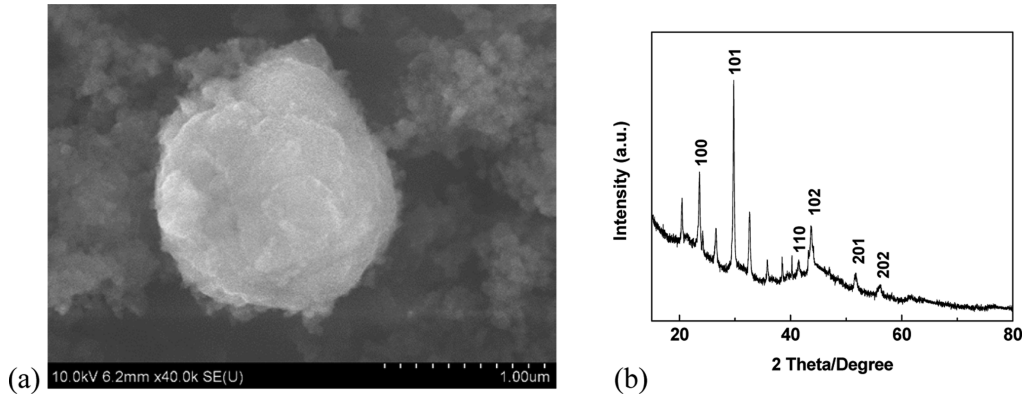

Figure 5. (a) SEM image and (b) XRD pattern of the Se/C composite after 1000 cycles in Li-ion batteries.

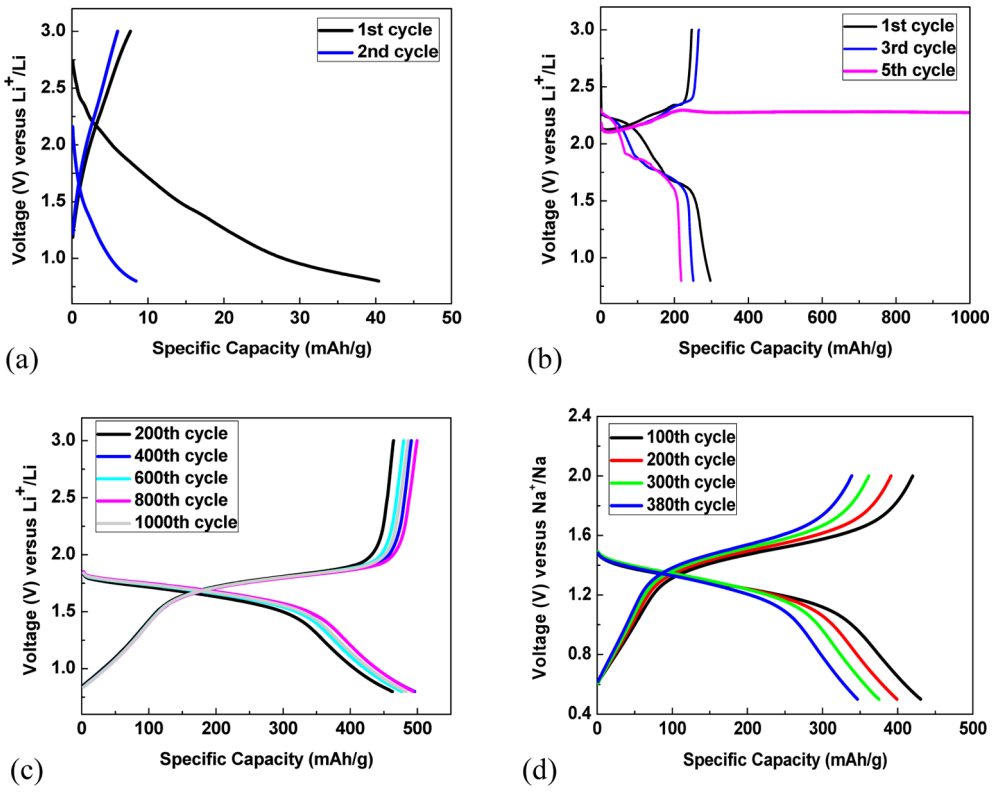

Figure 6. Charge/discharge profiles of pristine Se in (a) $LiPF_6$-EC/DEC electrolyte and (b) LiTFSI-TEGDME electrolyte. Charge/discharge profiles of Se/C composite in $LiPF_6$-EC/DEC electrolyte for (c) Li-ion batteries and (d) Na-ion batteries.

The mechanism behind the exceptional cycling stability and high Coulombic efficiency of the Se_8/C composite was investigated by comparing with the electrochemical performance of the pristine Se_{12} in the same electrolyte ($LiPF_6$-EC/DEC). The pristine Se_{12} electrode was prepared by mixing Se_{12} with carbon black and binder at a component ratio of 80:10:10 (Se/carbon black/binder). The charge/discharge behaviors of Se_{12} electrodes are presented in Figure 6. Only very short sloping lines can be observed in the charge/discharge curves, leading to a very low capacity of 10 mAh g^{-1}, which is 48 times less than that of Se_8/C electrodes. The side reaction between Li_xSe and the carbonate electrolyte for the less protective Se_{12}/carbon black composite[24] and large particle size of Se_{12} may be responsible for the low capacity. It has been proposed that use of high soluble electrolyte can improve the utilization of insulating S cathode, thus leading to high capacity.[8] Liquid electrolyte (LiTFSI in TEGDME) which has higher solubility for polysulfides than conventional carbonate electrolyte ($LiPF_6$ in EC/DEC) is employed for the Se cathode.[8] The Se_{12}/carbon black cathode in LiFTSI-TEGDME electrolyte shows two plateaus at 2.2 and 1.8 V (shown in Figure 6b). The two plateau reaction was also observed for Se/C cycling with LiTFSI in DOL/DME electrolyte by Cui *et al.*[25] The lithiation plateau at a high potential of 2.2 V is attributed to reduction of Se to the soluble polyselenides, Li_2Se_n ($n \geq 4$), while the plateau at a low potential of 1.8 V is

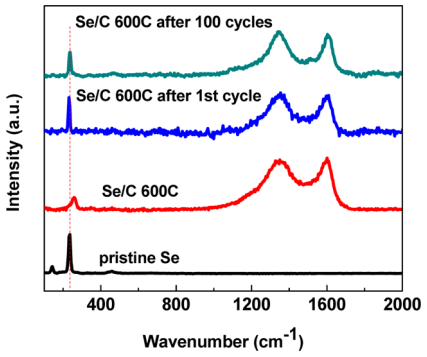

Figure 7. Raman spectra of pristine Se, Se/C composite before test, after first cycle, and after 100 cycles.

due to further reduction of soluble Li_2Se_n ($n \geq 4$), to nonsoluble Li_2Se_2, and Li_2Se.[25] During the delithiation, Li_2Se is first oxidized to Se_n^{2-} ($n \geq 4$), and then the high-order polyselenide is further oxidized to Se.[25] The high solubility of polyselenides in liquid LiTFSI-TEGDME electrolyte enhances the utilization of Se_{12}, thus increasing the capacity to more than 200 mAh g^{-1} (Figure 6b), which is more than 20 times higher than that in $LiPF_6$-EC/DEC electrolyte. However, the high solubility of polyselenides in the LiTFSI-TEGDME electrolyte also causes severe shuttle reaction, as evidenced by the endless voltage plateau at 2.2 V. Since the mesoporous carbon host can reduce the side reaction between Li_xSe and carbonate electrolyte and the stable Se−O layer formed on Li_xSe can protect Li_xSe

from further side reaction (Se−O layer function as a SEI), the low-cost $LiPF_6$-EC/DEC electrolyte can be used for the Se/C cathode, which is prepared by infusing Se into mesoporous carbon at a high temperature.

The ideal structure of Se/C nanocomposite has been realized by infusing Se into mesoporous carbon at a temperature of 600 °C. The exceptional electrochemical performance of the Se/C composite in $LiPF_6$-EC/DEC electrolyte (Figure 6c,d) is due to the uniform distribution of nano-Se_8 in porous carbon and direct generation of insoluble polyselenides. Structure change of Se during charge/discharge cycles in a Li-ion battery was measured using Raman spectroscopy. The Raman measurement for the Se/C composite before cycling and after 1 and 100 cycles is shown in Figure 7. The molecular structure of fresh Se in mesoporous carbon is ring-structured Se_8. The ring-structured Se_8 is converted to chain-structured Se_n after the first cycle, which is confirmed by the sharp peak at 235 cm^{-1} in the Raman spectrum. It retains chain-structured Se_n after 100 cycle. The similar result is also reported in the work by Yang *et al.*[24] It is believed that the formation of chain-structured Se_n after the first cycle leads to the high electrochemical stability of the Se/C composite.

CONCLUSION

Nano-Se_8-impregnated mesoporous carbon composites for Li-ion and Na-ion batteries are synthesized by infusing Se into mesoporous carbon at 600 °C under vacuum. Mesoporous carbon is employed to constrain Se_8 in its small pores to alleviate the shuttle effect. The Se_8/C composite cathode in both Li-ion and Na-ion batteries exhibits excellent electrochemical performance in low-cost carbonate-based electrolyte. The Se8/C in Li-ion batteries can deliver a reversible capacity of 480 mAh g^{-1} and maintains 1000 cycles without any capacity loss. The initial capacity of the Se/C composite for sodium-ion batteries is as high as 485 mAh g^{-1} and maintains 340 mAh g^{-1} after 380 cycles. The excellent battery performance of the Se/C composite is due to (1) use of small molecular Se_8 and its uniform distribution in mesoporeous carbon which allows most Se_8 molecules to react with Li ions and to protect Li_xSe from side reaction with carbonate electrolyte; (2) use of low-solubility and low-cost $LiPF_6$ in EC/DEC electrolytes which mitigate the dissolution of polyselenides. The exceptional electrochemical performance of the Se/C composite enables its application in lithium/sodium-ion batteries.

METHODS

Synthesis of Mesoporous Carbon Spheres. All chemicals were purchased from Sigma Aldrich and used as received. Resorcinol (R, 0.66 g), triblock copolymer (Pluronic F127, 0.38 g) and HCl aqueous solution (0.66 g) were dissolved in a mixture of 4.35 g of distilled water and 5.75 g of ethanol alcohol, where triblock copolymer and HCl functioned as soft template and catalyst, respectively. When a clear solution appeared, 0.8 g of 37% formaldehyde (F) aqueous solution was added. After 1 h of vigorous stirring, the solution was transferred into a Teflon-lined autoclave and sealed. It was heated to 150 °C and maintained for 10 h. After being naturally cooled to room temperature, a light brown powder was collected and dried in air for 24 h, and then followed by further curing in an oven at 100 °C for 24 h in air. Finally, the resulting precursor was carbonized in flowing argon at 600 °C for 5 h, with a heating ramp of 2 °C min^{-1} to achieve mesoporous carbon spheres.

Synthesis of Selenium-Impregnated Carbon Composite. Selenium and mesoporous carbon were mixed in a ratio of 1:1 by weight and sealed in a glass tube under vacuum. The sealed glass tube was annealed in an oven at 600 °C for 5 h. Selenium-impregnated carbon composite was collected as black powder.

Material Characterizations. Scanning electron microscopy (SEM) images were taken by Hitachi SU-70 analytical ultrahigh resolution SEM (Japan); transmission electron microscopy (TEM) images were taken by JEOL (Japan) 2100F field emission TEM; thermogravimetric analysis (TGA) was carried out using a thermogravimetric analyzer (TA Instruments, USA) with a heating rate of 10 °C min^{-1} in argon; X-ray diffraction (XRD) pattern was recorded by a Bruker Smart1000 (Bruker AXS Inc., USA) using Cu Kα radiation; BET specific surface area and pore size and volume were analyzed using N_2 absorption on Micromeritics ASAP 2020 (Micromeritics Instrument Corp., USA). Raman measurements were performed on a Horiba Jobin Yvon Labram Aramis using a 532 nm diode-pumped solid-state laser, attenuated to give ~900 μW power at the sample surface.

Electrochemical Measurements. The selenium-impregnated carbon composite was mixed with carbon black and sodium alginate binder to form a slurry at the weight ratio of 80:10:10. The electrode was prepared by casting the slurry onto aluminum foil using a doctor blade and dried in a vacuum oven at 60 °C overnight. The same method was used to fabricate pure selenium electrode material. Coin cells for lithium−selenium batteries were assembled with lithium foil as the counter electrode, 1 M $LiPF_6$ in a mixture of ethylene carbonate/diethyl carbonate (EC/DEC, 1:1 by volume) or 1 M LiTFSI in tetraethylene glycol dimethyl ether (TEGDME) as the electrolyte, and Celgard3501 (Celgard, LLC Corp., USA) as the separator. Coin cells for sodium−selenium batteries were assembled with sodium foil as the counter electrode, 1 M $NaClO_4$ in a mixture of ethylene carbonate/dimethyl carbonate (EC/DMC, 1:1 by volume) as the electrolyte, and Celgard3501 (Celgard, LLC Corp., USA) as the separator. Cells with pure selenium electrodes were also fabricated using the same procedure. Electrochemical performance was tested using an Arbin battery test station (BT2000, Arbin Instruments, USA). Capacity was calculated on the basis of the mass of selenium in selenium-impregnated carbon composites. Cyclic voltammogram was recorded using the Solatron 1260/1287 electrochemical interface (Solartron Metrology, UK) with a scan rate of 0.1 mV/s.

Conflict of Interest: The authors declare no competing financial interest.

Acknowledgment. This work was supported by the Army Research Office under Contract No. W911NF1110231. We acknowledge the support of the Maryland NanoCenter and its NispLab. The NispLab is supported in part by the NSF as a MRSEC Shared Experimental Facility.

Supporting Information Available: Additional figures. This material is available free of charge *via* the Internet at http://pubs.acs.org.

REFERENCES AND NOTES

1. Liu, C.; Li, F.; Ma, L.; Cheng, H. Advanced Materials for Energy Storage. *Adv. Mater.* **2010**, *22*, E28–E62.
2. Ellis, B. L.; Lee, K. T.; Nazar, L. F. Positive Electrode Materials for Li-Ion and Li-Batteries. *Chem. Mater.* **2010**, *22*, 691–714.

3. Kang, B.; Ceder, G. Battery Materials for Ultrafast Charging and Discharging. *Nature* **2009**, *458*, 190–193.
4. Ellis, B. L.; Nazar, L. F. Sodium and Sodium-Ion Energy Storage Batteries. *Curr. Opin. Solid State Mater. Sci.* **2012**, *16*, 168–177.
5. Bruce, P. G.; Freunberger, S. A.; Hardwick, L. J.; Tarascon, J. Li-O_2 and Li-S Batteries with High Energy Storage. *Nat. Mater.* **2012**, *11*, 19–29.
6. Guo, J.; Xu, Y.; Wang, C. Sulfur-Impregnated Disordered Carbon Nanotubes Cathode for Lithium Sulfur Batteries. *Nano Lett.* **2011**, *11*, 4288–4294.
7. Wang, H.; Yang, Y.; Liang, Y.; Robinson, J. T.; Li, Y.; Jackson, A.; Cui, Y.; Dai, H. Graphene-Wrapped Sulfur Particles as a Rechargeable Lithium Sulfur Battery Cathode Material with High Capacity and Cycling Stability. *Nano Lett.* **2011**, *11*, 2644–2647.
8. Zhang, S. S. Liquid Electrolyte Lithium/Sulfur Battery: Fundamental Chemistry, Problems, and Solutions. *J. Power Sources* **2013**, *231*, 153–162.
9. Akridge, J. R.; Mikhaylik, Y. V.; White, N. Li/S Fundamental Chemistry and Application to High-Performance Rechargeable Batteries. *Solid State Ionics* **2004**, *175*, 243–245.
10. Lu, X.; Kirby, B. W.; Xu, W.; Li, G.; Kim, J. Y.; Lemmon, J. P.; Sprenkle, V. L.; Yang, Z. Advanced Intermediate-Temperature Na−S Battery. *Energy Environ. Sci.* **2013**, *6*, 299–306.
11. Wang, D.; Zeng, Q.; Zhou, G.; Yin, L.; Li, F.; Cheng, H.; Gentle, I. R.; Lu, G. Q. Carbon/Sulfur Composites for Li−S Batteries: Status and Prospects. *J. Mater. Chem. A* **2013**, *1*, 9382–9394.
12. Ji, X.; Lee, K. T.; Nazar, L. F. A Highly Ordered Nanostructured Carbon−Sulphur Cathode for Lithium−Sulphur Batteries. *Nat. Mater.* **2009**, *8*, 500–506.
13. Zhang, B.; Qin, X.; Li, G. R.; Gao, X. P. Enhancement of Long Stability of Sulfur Cathode by Encapsulating Sulfur into Micropores of Carbon Spheres. *Energy Environ. Sci.* **2010**, *3*, 1531–1537.
14. Xin, S.; Gu, L.; Zhao, N.; Yin, Y.; Zhou, L.; Guo, Y.; Wan, L. Smaller Sulfur Molecules Promise Better Lithium−Sulfur Batteries. *J. Am. Chem. Soc.* **2012**, *134*, 18510–18513.
15. Suo, L.; Hu, Y.; Li, H.; Armand, M.; Chen, L. A New Class of Solvent-in-Salt Electrolyte for High-Energy Rechargeable Metallic Lithium Batteries. *Nat. Commun.* **2013**, *4*, 1481–1489.
16. Shin, E. S.; Kim, K.; Oh, S. H.; Cho, W. I. Polysulfide Dissolution Control: The Common Ion Effect. *Chem. Commun.* **2013**, *49*, 2004–2006.
17. Abouimrane, A.; Dambournet, D.; Chapman, K. W.; Chupas, P. J.; Weng, W.; Amine, K. A New Class of Lithium and Sodium Rechargeable Batteries Based on Selenium and Selenium−Sulfur as a Positive Electrode. *J. Am. Chem. Soc.* **2012**, *134*, 4505–4508.
18. Poborchii, V. V. Raman Spectra of Sulfur, Selenium or Tellurium Clusters Confined in Nano-Cavities of Zeolite A. *Solid State Commun.* **1998**, *107*, 513–518.
19. Lukács, R.; Veres, M.; Shimakawa, K.; Kugler, S. On Photo-induced Volume Change in Amorphous Selenium: Quantum Chemical Calculation and Raman Spectroscopy. *J. Appl. Phys.* **2010**, *107*, 073517-1-5.
20. Lin, Z.; Wang, Z.; Chen, W.; Lir, L.; Li, G.; Liu, Z.; Han, H.; Wang, Z. Absorption and Raman Spectra of Se_8-Ring Clusters in Zeolite 5A. *Solid State Commun.* **1996**, *100*, 841–843.
21. Guo, J.; Sun, A.; Chen, X.; Wang, C.; Manivannanb, A. Cyclability Study of Silicon−Carbon Composite Anodes for Lithium-Ion Batteries Using Electrochemical Impedance Spectroscopy. *Electrochim. Acta* **2011**, *56*, 3981–3987.
22. Guo, J.; Liu, Q.; Wang, C.; Zachariah, M. R. Interdispersed Amorphous MnO_x−Carbon Nanocomposites with Superior Electrochemical Performance as Lithium-Storage Material. *Adv. Funct. Mater.* **2012**, *22*, 803–811.
23. Xu, Y.; Zhu, Y.; Liu, Y.; Wang, C. Electrochemical Performance of Porous Carbon/Tin Composite Anodes for Sodium-Ion and Lithium-Ion Batteries. *Adv. Energy Mater.* **2013**, *3*, 128–133.
24. Yang, C.; Xin, S.; Yin, Y.; Ye, H.; Zhang, J.; Guo, Y. An Advanced Selenium−Carbon Cathode for Rechargeable Lithium Selenium Batteries. *Angew. Chem., Int. Ed.* **2013**, *52*, 8363–8367.
25. Cui, Y.; Abouimrane, A.; Lu, J.; Bolin, T.; Ren, Y.; Weng, W.; Sun, C.; Maroni, V. A.; Heald, S. M.; Amine, K. (De)Lithiation Mechanism of Li/SeS_x (x = 0−7) Batteries Determined by *In Situ* Synchrotron X-ray Diffraction and X-ray Absorption Spectroscopy. *J. Am. Chem. Soc.* **2013**, *135*, 8047–8056.
26. Slater, M. D.; Kim, D.; Lee, E.; Johnson, C. S. Sodium-Ion Batteries. *Adv. Funct. Mater.* **2013**, *23*, 947–958.